Report Title:	Additive Manufacturing of Energy Harvesting Material System for Active Wireless MEMS Sensors
Type of Report:	Final
Reporting Period:	September 2016 – August 2020
Principal Author:	Yirong Lin, PhD
Date Report Issued:	December 16, 2020
DOE Award Number:	DE-FE0027502
Submitting Organization:	**The University of Texas at El Paso** 500 W. University, ENG. Annex Suite - A111 El Paso, TX 79968

Disclaimer:

This report was prepared as an account of work sponsored by an agency of the United States Government. Neither the United States Government nor any agency thereof, nor any of their employees, makes any warranty, express or implied, or assumes any legal liability or responsibility for the accuracy, completeness, or usefulness of any information, apparatus, product, or process disclosed, or represents that its use would not infringe privately owned rights. Reference herein to any specific commercial product, process, or service by trade name, trademark, manufacturer, or otherwise does not necessarily constitute or imply its endorsement, recommendation, or favoring by the United States Government or any agency thereof. The views and opinions of authors expressed herein do not necessarily state or reflect those of the United States Government or any agency thereof.

Abstract

Combustion systems make up a large sum of the world's yearly energy production despite advances in renewable energy sources. Precise control of pressure and temperature in combustion chambers allows for lower carbon emissions, and overall higher efficiency. Wireless temperature and pressure sensors are critical for the operation of combustion chambers. Energy harvesters have emerged as a viable way to power wireless sensors when heat and mechanical energy are available. Lithium niobate (LNB), barium titanate (BTO), and lead zirconate titanate (PZT) pyroelectric ceramics were studied and fabricated through additive manufacturing (AM) for use as energy harvesting structures in combustion environments. The electric power generation potential of LNB and PZT ceramics was studied by varying the temperature from 50 to 60 °C and by introducing cyclic compression loads of 2000 N amplitude. It was found that thermal energy conversion had the highest output of 500 nW and that combined thermal and mechanical conversion did not increase the harvesting potential because of the competing contributions of both effects. Powder bed and slurry extrusion AM methods were used to fabricate BTO and PZT ceramic structures. Optimization of the powder-based binder jetting method produced BTO ceramics with a relative density of 36.77% a piezoelectric coefficient of 153 pC/N. The density of the ceramics increased up to 56% when increasing the saturation of binder in the powder to because of liquid phase sintering. Finally, PZT structures were manufactured through AM and fin features were added to the design to enhance the heat transfer along the material. The harvested power density of the flat samples was 3.643 $\mu W/cm^3$ and of the finned samples was 3.034 $\mu W/cm^3$. This research paves the ways for the development of self-powered wireless sensors in critical areas of operation such as combustion.

Table of Contents

Abstract iii

Table of Contents iiv

List of Tables vi

List of Figures vii

Chapter 1 Introduction and Background 1

1.1 Introduction 1

1.2 Background 2

1.2.1 Energy Harvesting in Combustion Systems 2

1.3 Objective 2

1.4 Literature Review 3

1.4.1 Thermal Energy Harvesting and Pyroelectric Effect 3

1.4.2 Mechanical Energy Harvesting and Piezoelectric Effect 5

1.4.3 Additive Manufacturing of Functional Ceramics 6

Chapter 2 Experimental Methodology and Technical Approaches 7

2.1 Additive Manufacturing of Energy Harvesting Ceramics 7

2.1.1 Binder Jetting Printing Process 8

2.1.2 Material Extrusion Printing Process 9

2.1.3 Binder Burnout and Sintering of 3D Printed Ceramics 11

2.1.4 Poling Process of 3D Printed Energy Harvesting Ceramics 12

2.1.5 Characterization Methods for Piezoelectric and Dielectric Properties of 3D Printed Ceramics 13

2.2 Thermal and Vibration Based Energy Harvesting 13

2.2.1 Characterization of Thermal Energy Harvesting of Pyroelectric Ceramics 13

2.2.2 Combined Thermal and Vibration Energy Harvesting with Pyroelectric/Piezoelectric Ceramics 15

Chapter 3 Results and Discussion 16

3.1 Additive Manufacturing of Energy Harvesting Ceramics 16

3.1.1 BTO Ceramics Fabricated through Binder Jetting 16

3.1.2 PZT Ceramics Fabricated through Material Extrusion 22

3.2 Thermal and Vibration Based Energy Harvesting Results 23
3.2.1 Thermal Energy Harvesting using LNB Ceramics 23
3.2.2 Combined Energy Harvesting Results 25
3.2.3 Thermal Energy Harvesting using AM Ceramics 28

Chapter 4 Conclusion 29

References 31

List of Tables

Table 2.1: Print parameters used in the Binder Jetting process 8
Table 2.2: Constituents of the paste used for Material Extrusion process.....10
Table 2.3: Print parameters for the Material Extrusion process 11
Table 2.4: Poling conditions for the energy harvesting ceramics.....12
Table 2.5: Poling conditions for the energy harvesting ceramics.....15

List of Figures

Figure 2.1: Schematic showing the binder jetting process .....**Error! Bookmark not defined.**
Figure 2.2: Schematic of the ME process for ceramic slurries 10
Figure 2.3: Sintering profile used for BTO and PZT ceramics. 12
Figure 2.4: Experimental setup for thermal energy harvesting characterization of LNB 14
Figure 2.5: Flat and finned PZT geometries fabricated through ME for energy harvesting characterization 14
Figure 2.6: Test fixture used for combined thermal and mechanical energy harvesting. 15
Figure 3.1: a) Front view of BTO coupons fabricated through binder jetting, b) Isometric view, c) Top view, d) Lattices structures of BTO fabricated through binder jetting process 17
Figure 3.2: SEM micrographs of printed BTO ceramics in plane perpendicular to print direction 18
Figure 3.3: SEM micrographs of printed BTO ceramics in plane parallel to print direction 18
Figure 3.4: Dielectric constant of printed BTO ceramics in paralell and perpendicular directions to the print direction 19
Figure 3.5: Piezoelectric coefficeint of printed BTO ceramics in paralell and perpendicular directions to the print direction 20
Figure 3.6: Elastic modulus and piezoelectric coefficient of the printed BTO ceramics in different arrangements 20
Figure 3.7: Modified sintering profile for BTO ceramics to promote liquid phase sintering 21
Figure 3.8: Densities of BTO ceramics with different binder saturations in the green body and sintered states 22
Figure 3.9: Finned and flat PZT ceramics fabricated through the ME process after sintering with coated silver electrodes 22
Figure 3.10: Developed pyroelectric current and induced temperature change on LNB ceramics in the temperature range of 75 to 100 °C 23
Figure 3.11: Pyroelectric coefficient measured for LNB ceramics under different temperature ranges 24
Figure 3.12: Harvested electrical power from LNB ceramics at different resistance loads and temeprature ranges 25
Figure 3.13: Peak power output from LNB ceramics at the range of temperature of 200 to 225 °C 25
Figure 3.14: Open circuit voltage generated by a PZT wafer subjected to cyclic compressive loads 26
Figure 3.15: Electric power output of PZT wafer under 2000 N cyclic compression at different electric loads 26
Figure 3.16: Electrical power harvested by PZT ceramics under hybrid mechanical and thermal loads across different external resistances 27
Figure 3.17: Power density of PZT structures fabricated through AM under varying electric loads 28

CHAPTER 1 INTRODUCTION AND BACKGROUND

1.1 Introduction

Combustion processes generate a large portion of the world's energy supply. Despite the growth of alternative energy sources, combustion is expected to make up 49% of the world's energy by 2050 [1] . Combustion processes require precise temperature and pressure conditions to ensure operational safety, maximum efficiency, and minimize carbon emissions. Temperatures must be maintained in a range of temperatures that promote efficient energy conversion while not exceeding the safety window of temperatures that could cause catastrophic failure. Because of their critical effects on combustion operation, temperatures and pressures must be constantly monitored throughout the complete life of the combustion chamber. In situ wireless sensors that can withstand the temperatures inside combustion chambers have been studied and their accuracy in monitoring temperature was demonstrated [2]. However, one remaining challenge for in situ sensors is their long-term operation inside of combustion chambers. A traditional process of removing the sensors once the on-board power supply is exhausted is costly as the combustion operation must be interrupted. Self-powered wireless sensors that can operate over long periods of years inside combustion chambers are an alternative that is safer and cheaper.

Self-powered wireless sensors are suitable in environments were easily obtainable energy is available. Combustion chambers offer high temperature fluctuations over time and mechanical vibrations that could be properly harvested using appropriate energy conversion mechanisms. Also, as sensors have miniaturized, eventually reaching Micro Electromechanical Systems (MEMS) scale, the energy required to power them also has also reduced. Current MEMS sensors require powers of only 1 to 20 μWs [3]. The operational environment of combustion chambers has sufficient available thermal and vibrational energy that could in theory be used to power any on board sensors. However, there exist only few material systems that can convert these environmental energies into useful electrical energy for operation. This study is interested in

developing materials suitable for harvesting thermal and vibrational energies in the harsh environments that combustion processes operate in.

1.2 Background

1.2.1 Energy Harvesting in Combustion Systems

There are various pathways towards harvesting energy in combustion environments. The available temperature gradients and mechanical loads can be converted into electrical energy through different methods including the thermoelectric effect, the thermionic effect, the pyroelectric effect, and the piezoelectric effect. The selected energy transfer mechanism must have high coefficients of energy conversion and high efficiencies in the selected operational environments. And the necessary materials must be inexpensive, processable, and able to withstand high temperatures and pressures.

Of the available energy transfer methods, the pyroelectric and the piezoelectric effects are most favorable. Pyroelectric energy conversion relies on immediate temperature gradients over time, which are widely available in combustion processes. Piezoelectrics are highly sensitive and can adequately convert the energy from dynamic mechanical loads. In many cases, pyroelectric ceramics are also piezoelectric, this opens the doors for combined energy harvesting with the use of a single component, reducing the complexity of the structures. Pyroelectric/piezoelectric ceramics also do not melt at temperatures required for combustion and are resistant to corrosion. However, one issue is that their functional range is limited by the temperatures at which crystallographic transitions occur. Thus, a limited selection of functional ceramics is available that can operate at the temperatures and pressures inside of combustion chambers. Despite this, this research project will study the use of functional ceramics to harvest environmental energies inside of combustion chambers using hybrid piezoelectric and pyroelectric effects.

1.3 Objective

The goal of this project is to develop hybrid thermal and vibrational energy harvesters capable of operating in the harsh environments present in combustion processes. These harvesters will in the future be mounted onto wireless sensors to provide long term operational life cycles.

First, energy harvesting ceramics will be developed using additive manufacturing (AM) processes that allow for complex geometries. Slurry and powder-based methods will be used to obtain ceramics with different degrees of porosities and geometrical resolutions. Different energy harvesting ceramics will be studied to demonstrate the capability of the AM processes to adapt to different materials. Electrically conductive fillers will be incorporated into the binding material of the powder-based process to enhance the final electromechanical properties of the parts and post processing conditions will be controlled to ensure quality parts are obtained.

Next, the hybrid energy harvesting capabilities of the manufactured ceramics will be evaluated by applying a change in temperature over time and a cyclic mechanical loading simultaneously. The energy harvesting performance will be evaluated by measuring produced power as well as by measuring the rate of voltage accumulation over time. The ceramics will be studied at different temperature ranges, and in environments with and without the presence of mechanical vibrations. The results from this objective will guide future design of MEMS wireless sensors with on-board energy harvesters suitable for combustion chambers.

1.4 LITERATURE REVIEW

1.4.1 Thermal Energy Harvesting and Pyroelectric Effect

Thermal energy from an environment can be harvested and used in a variety of manners [4]. For example, thermal energy can be directly used to heat other sections of a system in a process of regenerative heating. It can also be converted into mechanical or electrical energy. Among the methods that can be used to convert thermal energy to electrical energy and power MEMS sensors there exist the thermoelectric effect, the thermionic and the pyroelectric effect. The thermoelectric and thermionic effects rely on a defined temperature gradient along the thickness of a semiconductor. The temperature gradient produces an electric potential that can then be used to

power a system. As combustion chambers operate at consistently high temperatures, there is a close to ever-present temperature difference between the inside of a combustion chamber and sections closer to the outside environment. Both spatial temperature gradient based effects can provide consistent energy generation, but their conversion efficiency is low [4]. In contrast, energy harvesters working under the pyroelectric effect rely on temperature gradients over time to produce AC electrical power. They have the advantages over spatial gradient harvesters of being able to harvest energy in environments where temperature fluctuates at different times. One other advantage is that pyroelectric harvesters exhibit mechanical energy conversion as well: through the piezoelectric effect [5]. Pyroelectric energy harvesters are suitable for environments where heat and vibrations are both present.

The pyroelectric effect is present in various materials that are ferroelectric. Ferroelectric materials possess a permanent dipole moment or polarization even when not in the presence of an electric field. The ferroelectric category of materials includes various polycrystalline ceramics and crystalline polymers. When certain ferroelectric materials are exposed to a change in temperature, their polarization changes and produces surface charges. Once pyroelectric materials are connected to an electrical circuit, the potential built on their surface results in a current that can be rectified and stored as electrical energy.

The relationship between the developed electrical current in a pyroelectric material and the change in temperature it experiences is described by the following expression.

$$I = pA\frac{dT}{dt} \tag{1}$$

Here, the electrical current I results from the change in temperature over time dT/dt multiplied by the electrode area A and the pyroelectric coefficient p in units of C/m^2K. The pyroelectric coefficient defines the magnitude of the developed current and thus a higher coefficient magnitude is sought to enhance the harvesting capabilities.

An important parameter that describes the performance of a pyroelectric energy harvester is its range of temperatures of operation. The range of temperatures at which pyroelectric energy harvesting is possible for a material is defined by the Curie point. The Curie point is the

temperature at which the crystal structure of a ferroelectric material switches to a non-ferroelectric state. When the switching occurs, the spontaneous polarization of the material is released, and thus pyroelectric behavior is lost. Most common ferroelectric materials have a Curie point that does not exceed 350 °C [6]. Lithium Niobate is among the materials with the highest Curie point of 1140 °C [7]. With appropriate shielding, this material can be adapted into high temperature systems and reliably harvest energy without losing its pyroelectric nature.

Pyroelectric materials are parallel plate capacitors that store electrical energy as a result of applied heat. The energy stored in a pyroelectric capacitor is defined by the following expression:

$$E = \frac{p^2 A d \Delta T^2}{2\varepsilon} \quad (2)$$

Where d is the thickness of the pyroelectric, ΔT is the starting and ending temperature, and ε is the permittivity of the pyroelectric material. From the relationship it can be extracted that to increase the maximum stored energy in a pyroelectric energy harvested, the pyroelectric coefficient must be increased, and the permittivity decreased. The relationship between the pyroelectric coefficient and the permittivity is defined as the pyroelectric figure of merit F_E [Ref]:

$$F_E = \frac{p^2}{\varepsilon} \quad (3)$$

The performance of different pyroelectric harvesting materials can be compared using F_E. Table 1 shows different pyroelectric materials that will be studied, their F_E reported, and their Curie points.

There exist techniques to obtain higher F_E in pyroelectric materials. These techniques focus mainly on the reduction of the permittivity of the material while maintaining high pyroelectric coefficients. Powder based AM methods produce ceramics with porosity even after post processing. These methods have the potential to result in pyroelectric harvesters with even better F_E than their bulk counterparts [8].

1.4.2 Mechanical Energy Harvesting and the Piezoelectric Effect

Pyroelectric materials also exhibit piezoelectric behavior. The piezoelectric effect describes a change in the electric polarization of a material because of mechanical straining. The pyroelectric coefficient of a material in fact is partly composed of piezoelectric contributions from

thermally induced strains, and the electrical polarization is also highly sensitive to strains induced by external mechanical loads. The relationship between an applied mechanical load and the induced change in polarization in a piezoelectric material is described by the following relationship:

$$D = d * T + \varepsilon_T * E \quad (4)$$

Here, the induced change in polarization D results from the interaction of the piezoelectric coefficient d in units of C/N and the applied stress T, while also stemming from electrostatic interactions between an applied electric field E and the permittivity of the material at zero stress ε_T.

Piezoelectric materials have a defined piezoelectric coefficient that describes the magnitude of the developed polarization stemming from an applied mechanical stress. The piezoelectric coefficients of the pyroelectric materials previously presented are shown in Table 2. The piezoelectric effect is lost once the Curie point is reached like the pyroelectric effect because of the transition to a non-ferroelectric state.

In the case of harvesting mechanical energy from a combustion chamber, the vibrations experienced by a harvester will have different frequencies. It is expected that the piezoelectric energy harvesters will operate under off resonance conditions. The mechanical energy harvesting performance of a piezoelectric material under off-resonance conditions is directly proportional to the piezoelectric figure of merit F_P described by the following relationship [5]:

$$F_P = \frac{d^2}{\varepsilon * tan\delta} \quad (5)$$

Here, F_P is dependent on the piezoelectric coefficient d, the permittivity ε, and the dielectric loss tan δ. Thus, to maximize the performance of a piezoelectric energy harvester, the piezoelectric coefficient must be high, while the permittivity and dielectric loss must be low.

1.4.3 Additive Manufacturing of Functional Ceramics

Additive manufacturing of ceramics has been heavily researched in recent years [9]. The benefits of AM in ceramics is not only the reduced need for machining and the increased

complexity of geometrical features, but also the capability to realize metamaterial lattices with designed properties such as high stiffness [10], or anisotropic piezoelectric behavior [11].

It has been previously discussed that the figure of merit of pyroelectric and piezoelectric energy harvesters scale inversely with permittivity. A pathway towards increased figures of merit is the introduction of a secondary phase that reduces permittivity in the ceramics such as polymers or porosity. Various methods of porosity introduction have been implemented into conventional ceramics processing such as sacrificial polymer spheres that are burned off during sintering [12]. AM always results in ceramics with some degree of porosity due to the binder materials used during the manufacturing [13]. Powder based AM methods for ceramics result in high degrees of porosities where the resulting pores are interconnected in all three spatial dimensions. Because of this, powder-based AM methods can be explored to obtain functional ceramic harvesters with enhanced figures of merit.

CHAPTER 2 EXPERIMENTAL METHODOLOGY AND TECHNICAL APPROACHES

The project consisted in two objectives. The first objective consisted in fabricating energy harvesting ceramics using binder jetting and material extrusion AM methods. The impact of manufacturing parameters and post processing on the final electromechanical properties was assessed. The second objective consisted in energy harvesting characterization of different types of ceramics under combined thermal and mechanical loads. AM ceramics were also evaluated and compared to conventional ceramics in their thermal energy harvesting behavior.

2.1 Additive Manufacturing of Energy Harvesting Ceramics

This section describes the manufacturing process of energy harvesting ceramics studied in this project. Next, the post processing conditions common to ceramics manufacturing such as binder burnout and sintering are described. Finally, the ferroelectric processing parameters and the characterization methods of electric and electromechanical properties are described.

2.1.1 Binder Jetting Manufacturing of Energy Harvesting Ceramics

Binder Jetting (BiJ) is a powder bed AM process where a binding material is selectively jetted onto the powder bed each layer to consolidate a 3D structure. The process is illustrated in figure 2.1. The powder bed is composed of a ceramic or metal that is bound by a polymer binder. First, powder from a feed is rolled onto the build bed to fill the space of one layer. Afterwards, the binder is jetted, and, in most cases, a heat lamp is used to cure the binder and consolidate the layer. Next, the build bed is lowered by a height of one layer and the process is repeated. The final parts are removed from the powder bed and then placed in an oven to finish the cure process of the binder and obtain strong green bodies for post processing.

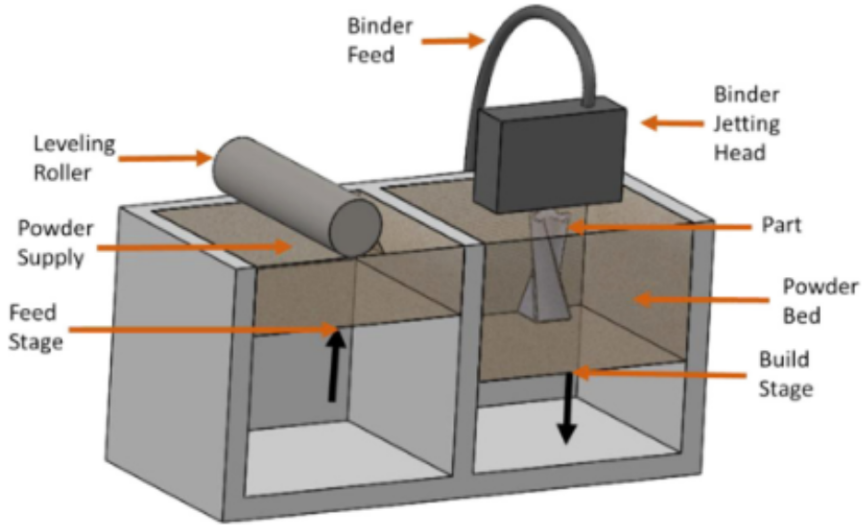

Figure 2.1. Schematic showing the binder jetting process.

There are various parameters that impact the quality of BiJ parts including powder parameters such as compaction, feed ratios, feed speeds, and layer heights, as well as parameters related to the binder such as saturation, curing temperatures, and heat exposure times. The print parameters used in this project are shown in table 2.1.

Parameter	Value
Powder packing rate (%)	24.4
Layer thickness (μm)	135

Binder saturation (%)	100
Feed to build ratio	1.75
Initial spread speed (mm/s)	5
Drying time (s)	120

Table 2.1. Print parameters used in Binder Jetting process.

The material selected for this project was barium titanate (BTO). This ceramic has a bulk pyroelectric coefficient on the order of 10^{-8} C/cm^{2}K [14], a piezoelectric coefficient of 190 C/N, and a relative permittivity of 1700 [15]. One drawback of this material is its low Curie point of 130 °C. However, it provides a starting point for the development of energy harvesting ceramics using AM.

2.1.2 Material Extrusion Manufacturing of Energy Harvesting Ceramics

A material extrusion (ME) process was also explored for the fabrication of energy harvesting ceramics. The ME method consists in the selective deposition through a nozzle of a ceramic filled slurry to form layers that consolidate into a 3D part. The process is illustrated in figure 2.2. The parameters that play a role in the ME process include the deposition rate, the printing speed, the nozzle diameter, and the layer height. Consolidation of the printed beads and shape retention are achieved through different means such as polymer network reformation [16] and drying [17].

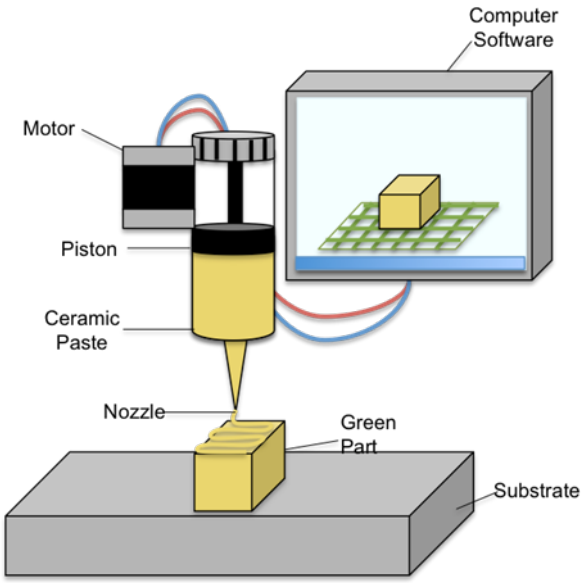

Figure 2.2. Schematic of the ME process for ceramic slurries.

The components of the ceramic slurry determine the rheological properties as well as the density of the final printed parts. Thus, appropriate control of the constituents is one of the biggest challenges in ME of ceramics. The components of the ceramic slurry often include the ceramic powder, a liquid medium, and organic additives such as binders, dispersants, plasticizers, and coagulants. The ceramic selected in this project for the ME process was lead zirconate titanate (PZT). This functional ceramic has superior pyroelectric and piezoelectric sensitivities when compared to BTO, and has a Curie point of above 300 °C. The specific PZT ceramic used in this study was a Navy Type II with a piezoelectric constant of 400 pC/N, a relative permittivity of 1900, and a Curie point of 360 °C. The particles were received from the manufacturer coated with polyvinyl alcohol (PVA) to act as a dispersant. The slurry was prepared with the coated ceramic particles, and a solution of additional PVA in deionized water to act as the liquid medium and binding agent. The mass ratios of the constituents of the slurry used for the ME process are shown in table 2.2 and the printing parameters used for the slurry are shown in table 2.3.

Constituent	**Mass (%)**
Ceramic	85.5

Binder	1.45
Water	13.05

Table 2.2 Constituents of the paste used for ME process.

Parameter	Value
Nozzle Diameter (mm)	0.41
Layer thickness (mm)	0.8
Print speed (mm/s)	5
Air pressure (psi)	60
Bed temperature (°C)	40

Table 2.3 Print parameters for the ME process.

2.1.3 Binder Burnout and Sintering of 3D Printed Ceramics

Ceramics produced by both the BiJ and ME processes are in the green body state where the individual particles are bound by organic binders and there is a high degree of porosity. Thus, the fabricated parts must be subject to processes of binder removal and sintering to achieve maximum density and electromechanical properties. The BTO and PZT parts were sintered according to schedule shown in figure 2.3. Holds were introduced at lower temperatures to ensure binder burnout, and at the higher, sintering temperatures to promote complete densification. PZT ceramics were sealed inside their alumina crucibles with a PZT powder cover before sintering to ensure no loss in lead content at high temperatures [18].

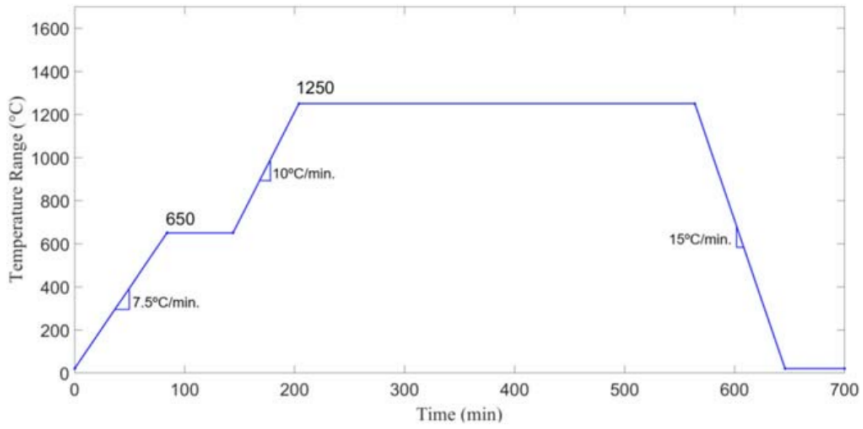

Figure 2.3. Sintering profile used for BTO and PZT ceramics.

2.1.4 Poling Process of 3D Printed Energy Harvesting Ceramics

After densification, the printed ceramics were electrically poled using a hot oil bath process. First, electrodes were deposited on the top and bottom surfaces using silver paint. Then, the parts were submerged in an oil bath and raised to their poling temperature. Once the temperature was reached, a DC electric field was applied to the parts and held some time to allow poling to occur. Once the time elapsed, the samples were cooled down to room temperature with the electric field still on to ensure the poling was not erased occurred during cooling. Finally, the electric field was switched off upon reaching room temperature. The poling conditions of the printed BTO and PZT ceramics are shown in table 2.4.

Material	Poling Temperature	Electric Field	Poling Time
BTO	60 °C	0.33 kV/mm	2 hours
PZT	100 °C	1 kV/mm	1 hour

Table 2.4. Poling conditions for the energy harvesting ceramics.

2.1.5 Characterization Methods for Piezoelectric and Dielectric Properties of 3D Printed Ceramics

The piezoelectric coefficient of the ceramics was measured using a d_{33} meter (Wide Range d_{33} Meter, APC International) in the 33 mode, which represents the piezoelectric response to loads in the same direction as the poling orientation.

The dielectric properties of the printed ceramics were measured using an LCR meter (1920 Precision LCR, IET Labs). The capacitance of the samples after poling was estimated at a quasistatic frequency of 1 kHz and then the relative permittivity was calculated based on the parallel plate capacitance relationship shown in equation 6.

$$C = \frac{k\varepsilon_0 A}{d} \tag{6}$$

Here, the relative permittivity k, can be obtained from the capacitance C, the permittivity of free space ε_0, the area of the electrodes A, and the thickness of the part d.

2.2 Thermal and Vibration Based Energy Harvesting

This section describes the test methods used to characterize the performance of energy harvesting ceramics. Conventionally manufactured lithium niobate (LBN) and PZT samples, as well as PZT samples fabricated through ME were characterized for their energy harvesting performance.

2.2.1 Characterization of Thermal Energy Harvesting of Pyroelectric Ceramics

The thermal energy harvesting performance of conventionally manufactured lithium niobate (LNB) and PZT samples, as well as PZT samples fabricated through ME was characterized using two different methods.

First, the performance of LNB wafers (Precision Micro-Optics LLC) with a diameter of 76.2 mm and a thickness of 0.5 mm was characterized using a custom-built heating setup as shown in figure 2.4.

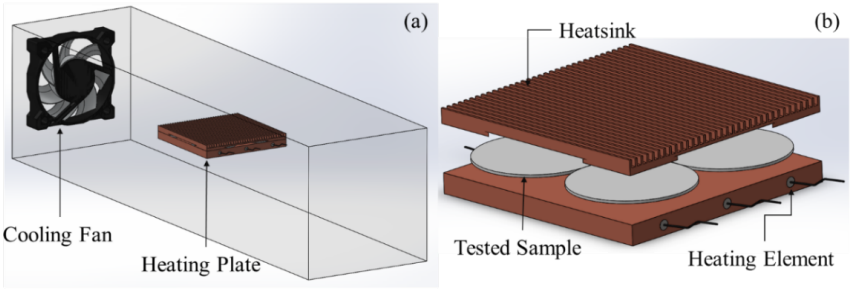

Figure 2.4. Experimental setup for thermal energy harvesting characterization of LNB.

The LNB wafers were heated using a heating plate and cooled through forced convention from a fan and with the aid of heat sinks. A microcontroller was used to carefully control the heating and cooling cycles. The temperature was cycled in 25 °C intervals starting at 75 °C and then raising the lower temperature until the upper temperature was 225 °C. The electrical current developed and the harvested power were measured by connecting the electrodes of the ceramics to an external load resistance.

Second, the pyroelectric energy harvesting performance of ME PZT structures was characterized using a similar approach. The different geometries studied are shown in figure 2.5. Structures with and without fins were compared as it was expected that the fins would increase the dissipation of heat and produce larger currents under the same applied heats. The printed structures were placed on Peltier heating plates and the temperature was continuously cycled by applying electrical power to the plates. This time, cooling was achieved through natural convection. Once again, the ceramics were connected to an external resistance and the power density of the different geometries was measured at varying loads.

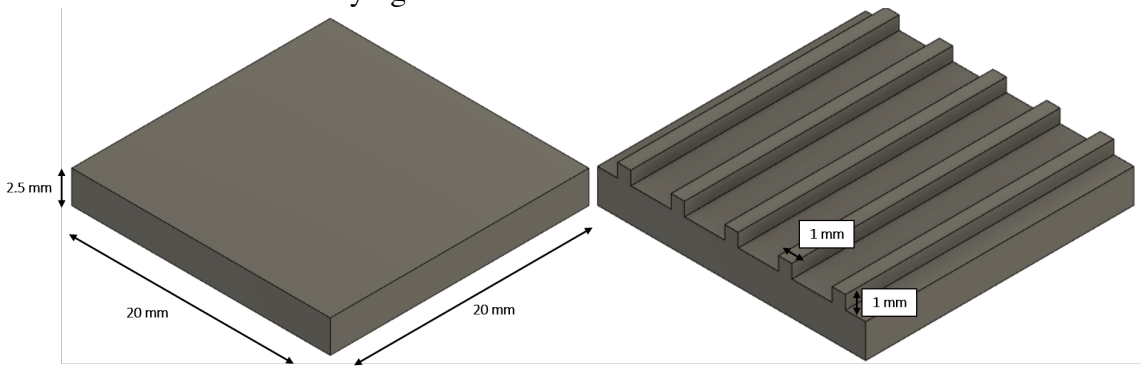

Figure 2.5. Flat and finned PZT geometries fabricated through ME for energy harvesting characterization.

2.2.2 Combined Thermal and Vibration Energy Harvesting with Pyroelectric/Piezoelectric Ceramics

A custom-built setup was used to characterize the energy harvesting performance of conventionally manufactured PZT ceramics under combined thermal and mechanical loading. First, mechanical test fixtures with temperature cycling capabilities were designed and machined out of Aluminum 6061 block as shown in figure 2.6. Finite element analysis was performed to ensure that it would not fail under the combined mechanical and thermal stresses expected during the test. The heating elements inserted into the fixture were controlled through a microcontroller receiving feedback from the thermocouple inserted.

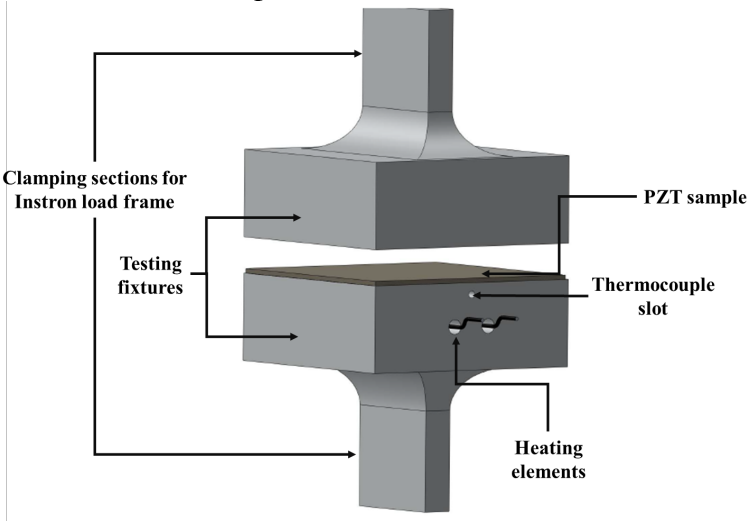

Figure 2.6. Test fixture used for combined thermal and mechanical energy harvesting.

Different testing conditions were used to characterize the energy harvesting of PZT under thermal, mechanical, and combined loading. A test matrix of the different conditions is shown table 2.5.

Test	Initial Mechanical Conditions	Initial Thermal Conditions	Mechanical Cycling Load	Thermal Cycling Load

Pure Mechanical	2500 N Compression	Room Temperature	1000 N Amplitude at 0.05 Hz	No Thermal Cycling
Pure Thermal	2500 N Compression	Room Temperature	No Cycling Load Applied	Temperature Cycled at 50 to 60 °C
Mechanical at 50 °C	2500 N Compression	50 °C	1000 N Amplitude at 0.05 Hz	Constant Temperature
Mechanical at 60 °C	2500 N Compression	60 °C	1000 N Amplitude at 0.05 Hz	Constant Temperature
Combined	2500 N Compression	Room Temperature	1000 N Amplitude at 0.05 Hz	Temperature Cycled at 50 to 60 °C

Table 2.5. Thermal and mechanical testing conditions used to characterize PZT

CHAPTER 3 RESULTS AND DISCUSSION

The results from the AM and energy harvesting characterization efforts are presented in this section. The feasibility of using AM to obtain functional ceramics for energy harvesting applications was demonstrated, and the features that arise from the manufacturing processes are discussed. The characterization of pyroelectric ceramics of PZT and LNN in thermal, mechanical, and combined load environments is shown and the performance in different environments is compared. The interaction of AM and energy harvesting is explored as well, showing the impact of using different geometries with features enabled by AM to increase energy harvesting potential.

3.1 Additive Manufacturing of Energy Harvesting Ceramics

3.1.1 BTO Ceramics Fabricated through Binder Jetting

BTO ceramics were successfully fabricated through BiJ AM process. Through control of manufacturing parameters such as the packing ratio, the binder saturation, the rolling speed, and the layer height an average green body density of 25.65% was obtained. After sintering, the density increased up to 36.77% with an average shrinkage of 20% in each axis observed. Photographs of

coupons fabricated using BiJ for electromechanical characterization portraying them before and after sintering are shown in figure 3.1. Included as well, are lattice structures of BTO enabled by BiJ that while not used for characterization showcase the potential of the AM technique to produce complex geometries with high resolution.

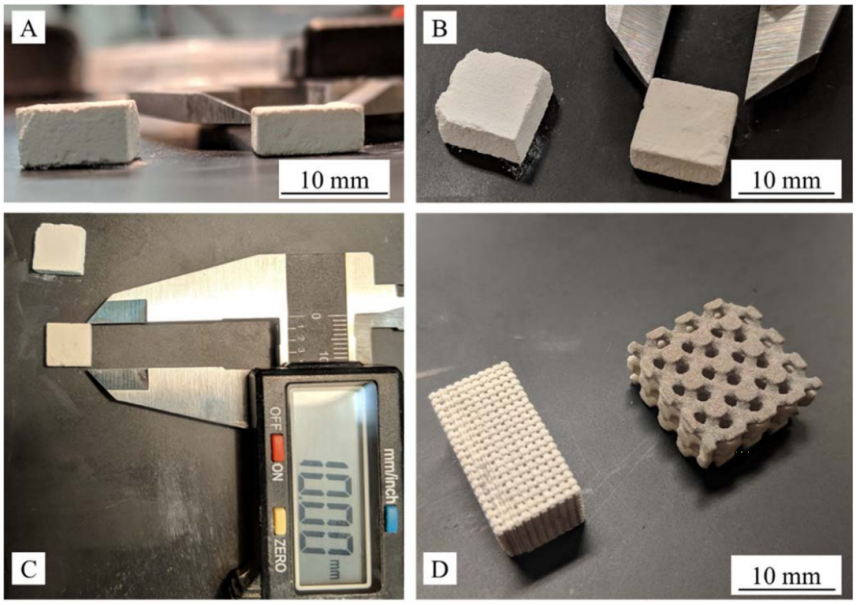

Figure 3.1. a) Front view of BTO coupons fabricated through binder jetting, b) Isometric view, c) Top view, d) Lattices structures of BTO fabricated through binder jetting process.

The pore morphology of the printed ceramics was next studied using SEM to observe the porosity resulting from the manufacturing process. In order to observe the internal features, the sintered BTO ceramics were grinded and polished in both the direction of printing and perpendicular to the direction of printing. Anisotropic degrees of porosity were expected due to the increased amount of binder along the print direction compared to the layer planes. The SEM images in figures 3.2 and 3.3 of the printed parts revealed that there is a high degree of porosity in both directions. The pores along the print direction had a patterned arrangement revealing the stacking of multiple layers to form the ceramic. In contrast, scans of the ceramics in the print direction showed less porosity in plane which agrees with higher packing inside of the layer of powder during the print process.

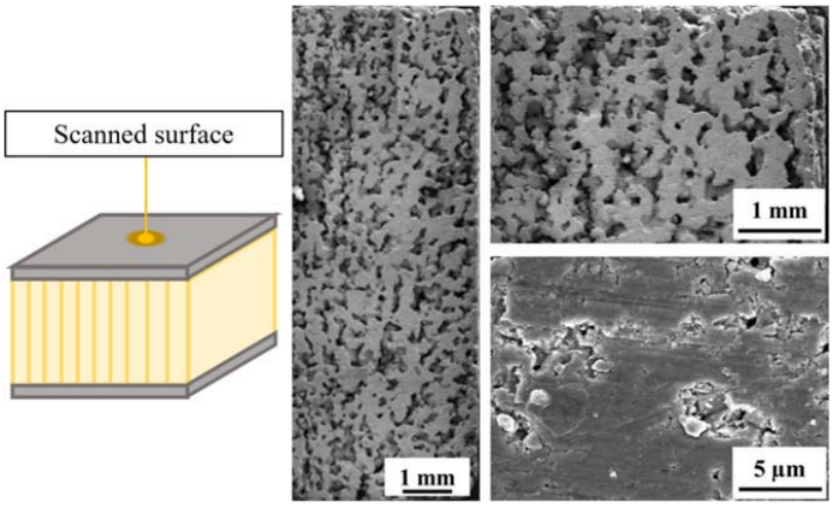

Figure 3.2. SEM micrographs of printed BTO ceramics in plane perpendicular to print direction.

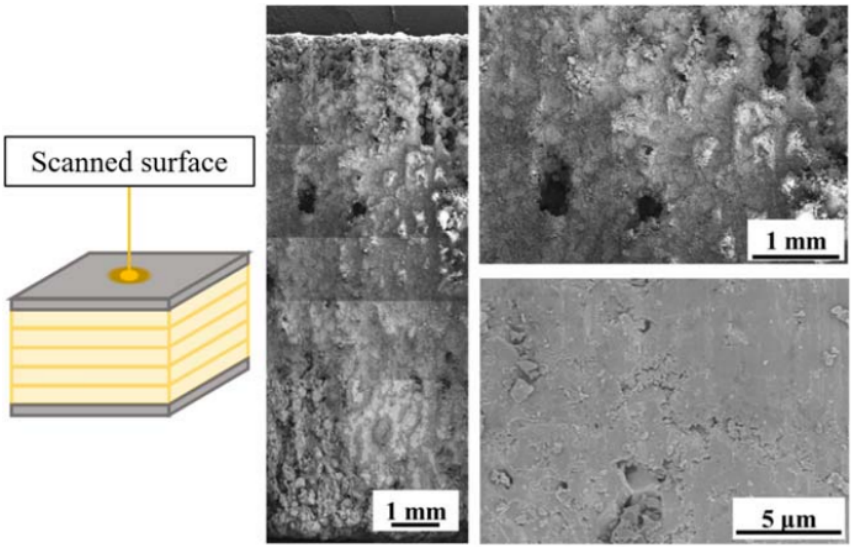

Figure 3.3. SEM micrographs of printed BTO ceramics in plane parallel to print direction.

The electromechanical properties of the BTO ceramics were characterized in arrangements perpendicular and parallel to the print direction to observe the differences in properties due to the different degrees of porosity. The relative permittivity of the samples was measured for the different arrangements and the results are shown in figure 3.4. An average permittivity of 581.6 was obtained parallel to the printed direction. In contrast, the parts tested perpendicular to the print orientation showed a permittivity of 698. The difference in permittivity of the two configurations could be explained from the arrangement of virtual capacitor networks of ceramic and air. In the

case of ceramics measured in the printing direction, the network of capacitors acts in series, with the layers of pores overall diminishing the capacitance of the ceramic. In the case of ceramics perpendicular to the print direction, the different capacitive layers of ceramic and air are arranged in a parallel and thus, the lower capacitance of the pores does not diminish the capacitive potential of the layers of ceramic.

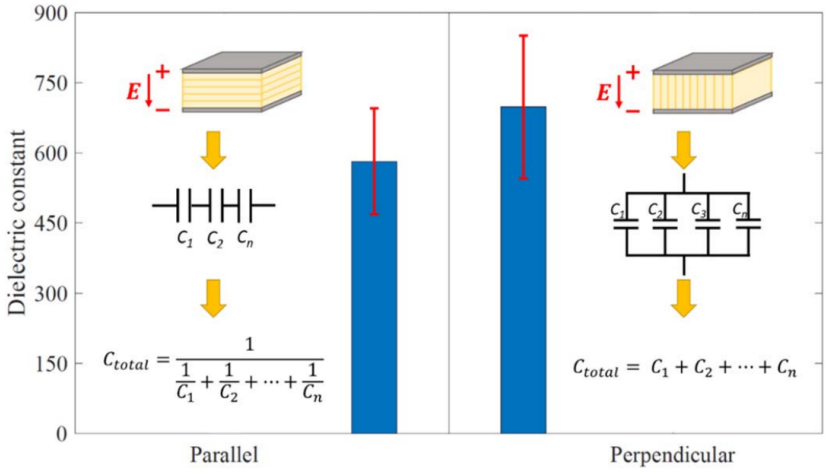

Figure 3.4. Dielectric constant of printed BTO ceramics in parallel and perpendicular directions to the print direction.

The piezoelectric coefficient of the ceramics was also evaluated in both perpendicular and parallel arrangements and the results are shown in figure 3.5. Once again, the perpendicular arrangement showed an increased piezoelectric constant compared to the parallel arrangement because of the arrangement of the porous layers. The parallel arrangement showed an average piezoelectric coefficient of 113 pC/N while the perpendicular arrangement showed a coefficient of 153 pC/N. The explanation for this phenomenon is that mechanical loads are better transferred in the perpendicular arrangement while in the parallel arrangement, air gaps in between layers dampen the transfer of energy and reduce the electromechanical energy conversion. The printed ceramics could not achieve the bulk piezoelectric coefficient of 190 pC/N observed for fully dense BTO ceramics, however, the reduced dielectric constant when compared to bulk means that the FOM was improved with respect to bulk ceramics.

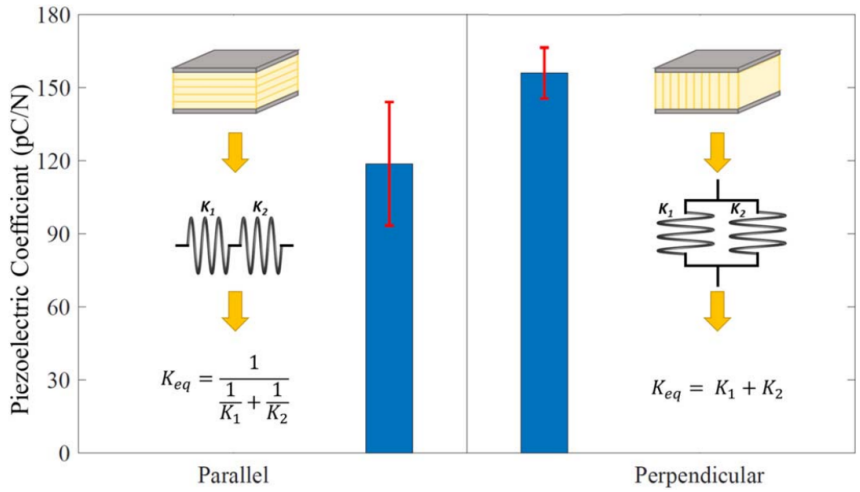

Figure 3.5. Piezoelectric coefficient of printed BTO ceramics in parallel and perpendicular directions to the print direction.

Compression testing was carried out to characterize the strength of BTO parts in both parallel and perpendicular arrangements. The results of the compressive modulus together with the piezoelectric coefficient are shown in figure 3.6. From the figure, it can be observed that the mechanical properties had a direct correlation to the electromechanical properties. The increased stiffness in the perpendicular arrangements increased the electromechanical energy conversion through enhanced load transfer.

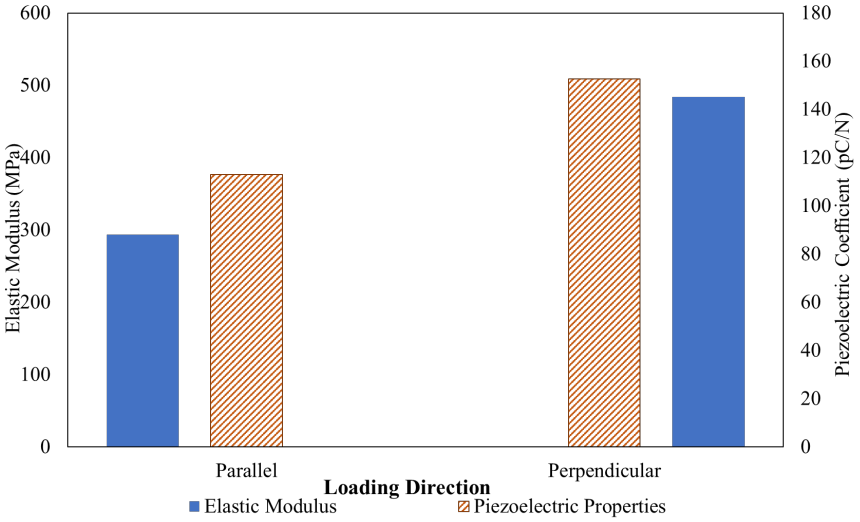

Figure 3.6. Elastic modulus and piezoelectric coefficient of the printed BTO ceramics in different arrangements.

Efforts were also done to optimize the BiJ printing process for BTO ceramics by varying the binder saturation level. The increase in binder concentration was expected to aid in the densification of the ceramic during the sintering process through what is known as liquid phase sintering [19]. In the process of liquid phase sintering, a liquid material redistributes the powder particles of the part and provides increased available surface energy that promotes grain fusion and densification. The binder saturation parameter during the print process was varied from the value of 100% used previously, and a modified sintering schedule was developed to promote binder liquefication and redistribution of ceramic particles. The modified sintering schedule is shown in figure 3.7.

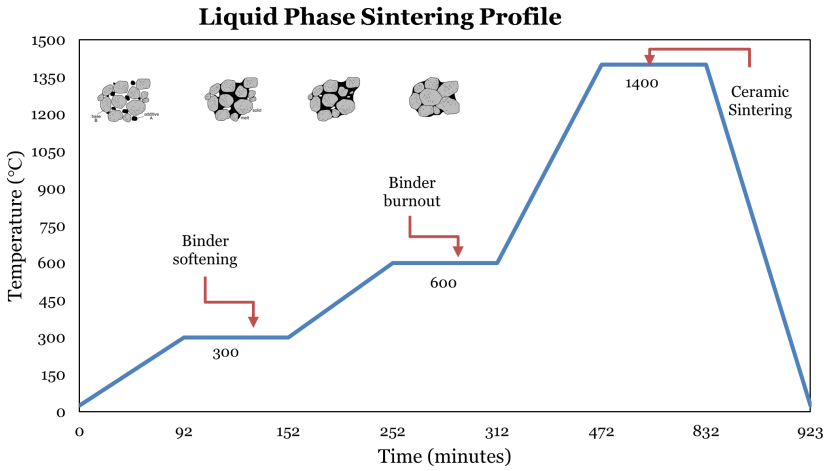

Figure 3.7. Modified sintering profile for BTO ceramics to promote liquid phase sintering.

Figure 3.8 shows the densities of BTO ceramics fabricated with increasing binder saturations from 115% up to 300%. The green body density showed a linearly increasing trend due to the binder occupying porosity in the ceramic. However, a clear trend was not observed for the final sintered density in all the cases. The increase in binder added during the AM process promoted liquid phase sintering and increased the overall density, but past a certain level of saturation, the increase in binder content could result in large separation between particles and a lower sintering overall. The highest density of sintered ceramics was found between 145% and 205% binder saturation.

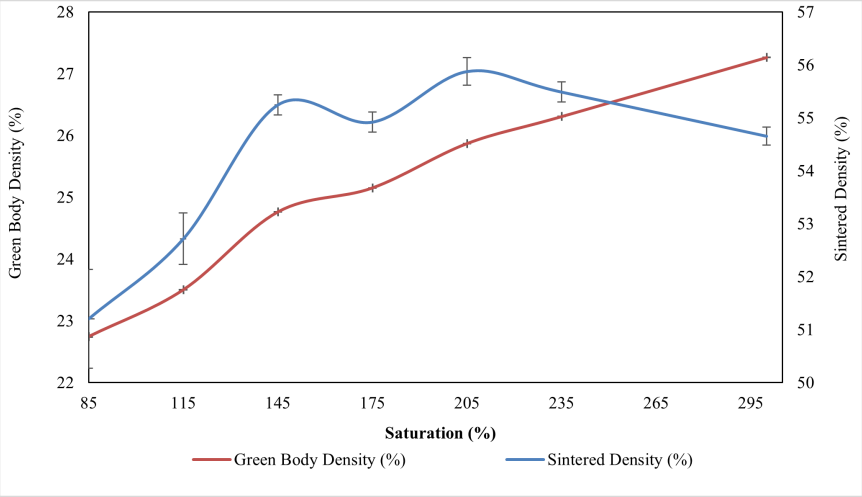

Figure 3.8. Densities of BTO ceramics with different binder saturations in the green body and sintered states.

3.1.2 PZT Ceramics Fabricated through Material Extrusion

PZT ceramics were fabricated through the method of ME to demonstrate the feasibility of other AM methods to fabricate functional parts for energy harvesting. Figure 3.9 shows finned and flat PZT energy harvesting structures fabricated through ME. These structures were used for thermal energy harvesting and compared against conventionally manufactured ceramics.

Figure 3.9. Finned and flat PZT ceramics fabricated through the ME process after sintering with coated silver electrodes.

3.2 Thermal and Vibration Based Energy Harvesting Results

This section presents the results from energy harvesting characterization of pyroelectric ceramics due to thermal and mechanical loads. LNB ceramics are characterized in thermal loading mode, while PZT ceramics are characterized in combined loads. AM structures are also compared to conventionally manufactured ceramics.

3.2.1 Thermal Energy Harvesting using LNB Ceramics

The thermal energy harvesting performance of LNB was characterized by introducing heat and measuring the generated electric current at different temperature ranges. Figure 3.10 shows a plot of the developed currents over time under a repeated cycle of heating and cooling. The developed current is in phase with the introduced temperature change, demonstrating the pyroelectric nature of the LNB ceramic.

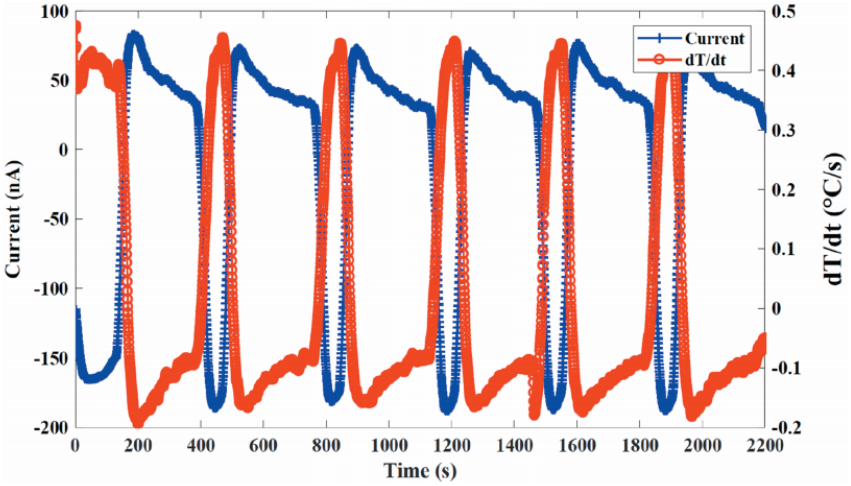

Figure 3.10. Developed pyroelectric current and induced temperature change on LNB ceramics in the temperature range of 75 to 100 °C.

The pyroelectric coefficient was estimated from the proportionality of the developed current and the observed temperature change. Values were measured in contained temperature ranges of 25 °C that began in the range of 75 °C to 100 °C and then raised up to 200 ° to 225 °C. The estimated pyroelectric coefficients are shown in figure 3.11. It is shown that the magnitude of the pyroelectric coefficient increased with temperature, which agrees with previously reported

behaviors for ferroelectric ceramics approaching the Curie temperature [Pyro Coefficient Ref]. A maximum pyroelectric coefficient of -196 μC/m^{2}K was found in the 200 to 225 °C, which represented a 96% increase when compared with room temperature pyroelectric coefficient of -100 μC/m^{2}K.

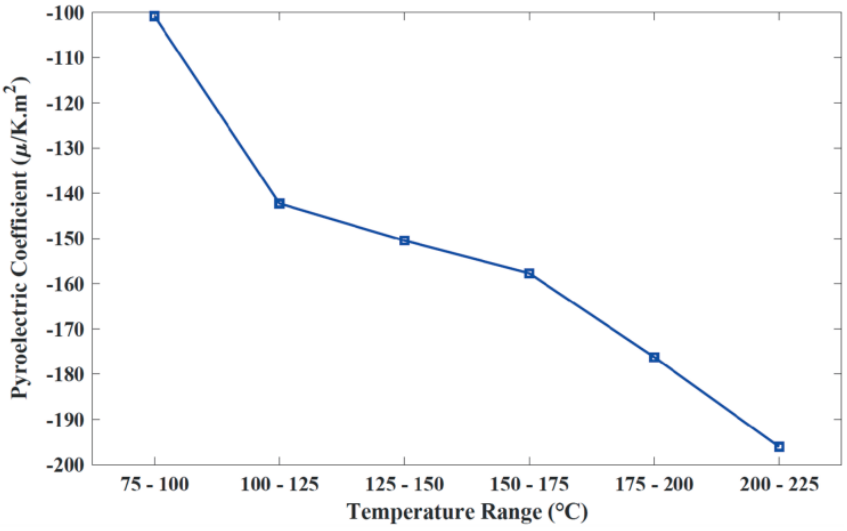

Figure 3.11. Pyroelectric coefficient measured for LNB ceramics under different temperature ranges.

The thermal energy harvesting capabilities of LNB were characterized by measuring the output power through an external electric load. The power generated was measured at different temperature ranges and the results are shown in figure 3.12. The output power decreased as temperature increased for two reasons. First, it was observed that under the same applied heat, the rate in temperature change decreased due to natural convection of heat to the environment slowing down the heating at higher temperatures. Also, the impedance of the LNB ceramics decreased with increasing temperatures, thus lowering the electrical resistance at maximum power transfer. For temperature ranges of 75 to 150 °C, the electrical power harvested increased by increasing the electrical resistance in the range of 100 to 1000 MΩ. A maximum harvested power of 20.5 μW in the range of electric loads was observed for the 75 to 100 °C range. However, in the range of 200 to 225 °C, despite the increased pyroelectric coefficient, the lower impedance and lower rate of temperature change resulted in a much lower power, with a peak output found below 100 MΩ. The

harvested power of the LNB at the high temperature range of 200 to 225 °C at low electric loads, showing the peak output is shown in figure 3.13.

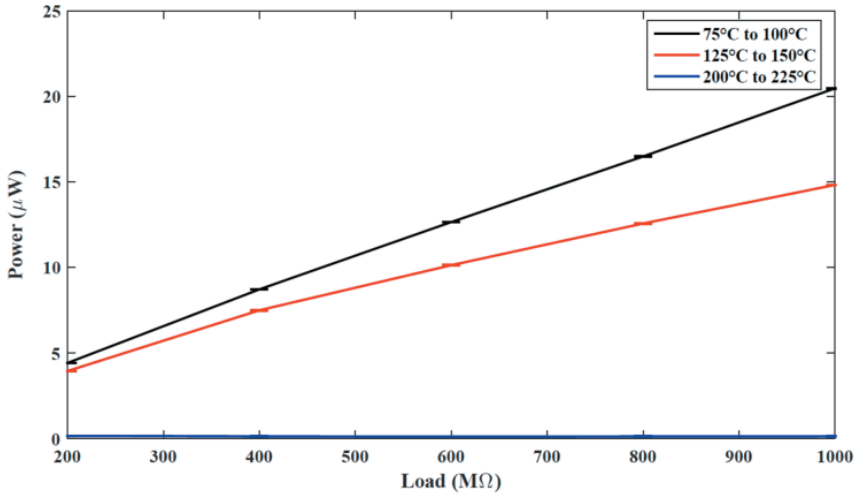

Figure 3.12. Harvested electrical power from LNB ceramics at different resistance loads and temperature ranges.

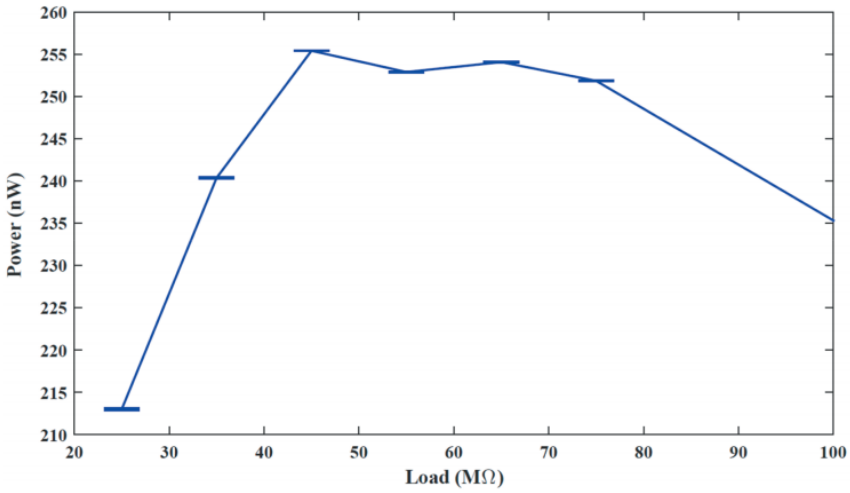

Figure 3.13. Peak power output from LNB ceramics at the range of temperatures of 200 to 225 °C.

3.2.2 Combined Energy Harvesting Results

The energy harvesting capabilities of PZT ceramics were evaluated under combined thermal and mechanical loads to make use of the pyroelectric and piezoelectric behaviors of the

ceramics. First, the PZT wafers were loaded under cyclic compression, and then heating was introduced into the testing arrangement.

The results from an open circuit measurement of generated voltage under cyclic mechanical loading are shown in figure 3.14. A peak-to-peak voltage of 15 V was measured when a cyclic compressive load of 2000 N was applied. The voltage generated was in phase and the results agreed with the theoretical properties of the piezoelectric ceramic.

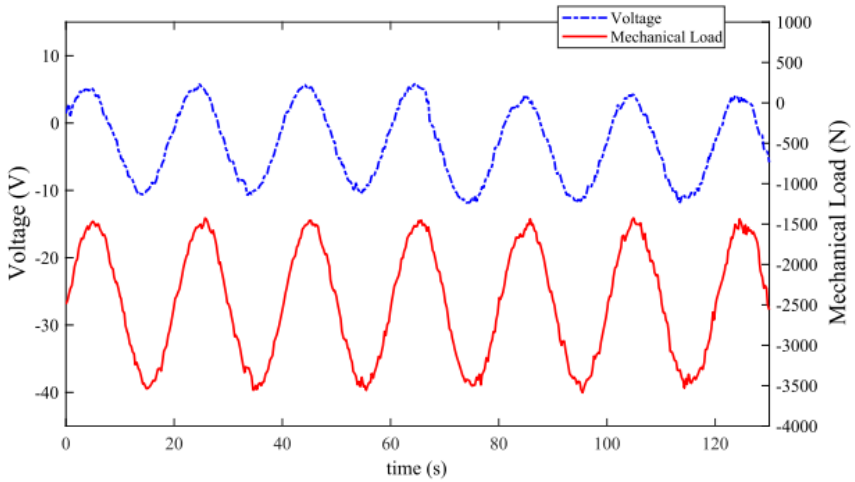

Figure 3.14. Open circuit voltage generated by a PZT wafer subjected to cyclic compressive loads.

Next, the power generation potential of the ceramic was evaluated under closed circuit conditions by using varying external electric loads. The output powers are shown in figure 3.15. Peak power was achieved at 10 MΩ electric load with a maximum power close to 30 nW.

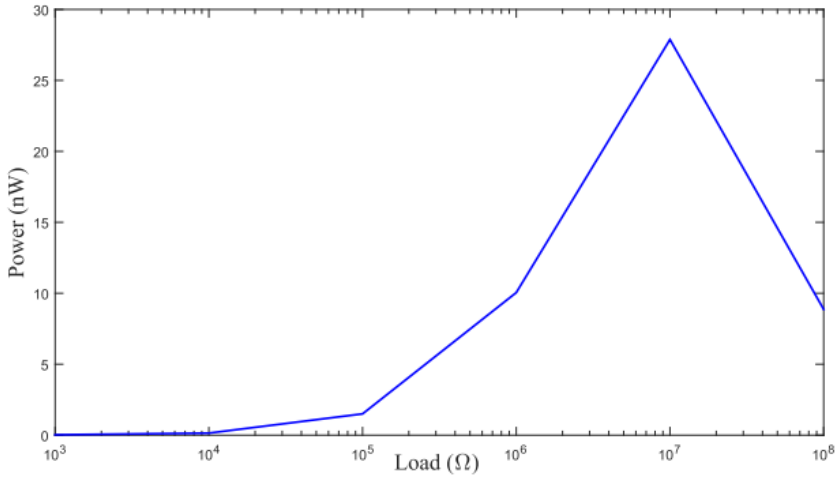

Figure 3.15. Electric power output of PZT wafer under 2000 N cyclic compression at different electric loads.

The thermal and combined mechanical energy harvesting performances of the PZT ceramics were evaluated according to the testing conditions defined in the methods section. The range of electrical loads were selected to be from 10 MΩ to 60 MΩ according to the value of peak power obtained from the mechanical energy harvesting tests. The power out puts of the different load conditions are shown in figure 3.16.

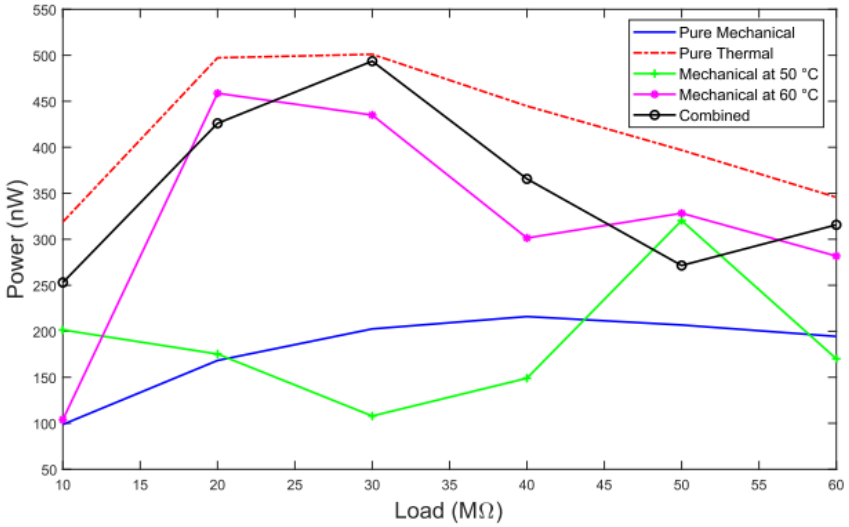

Figure 3.16. Electrical power harvested by PZT ceramics under hybrid mechanical and thermal loads across different external resistances.

The lowest power generated was under pure mechanical conditions. The power then increased as the environmental temperature increased from 50 to 60 °C. This can be explained as the piezoelectric coefficient of PZT increased by approaching the Curie point. The pure thermal loads, when cycling from 50 to 60 °C produced the highest power out of all arrangements. Even higher than the power outputted under combined loads. The reason for the lower power under combined loads is that the frequencies of mechanical loads and temperature changes are out of phase, thus having competing effects on the dipole motions at any point in time.

Regardless, the energy harvesting capabilities under combined loads, and different temperature and mechanical conditions for PZT ceramics was demonstrated. Further work needs to be done in order to find optimal interactions of the load with the energy harvesting ceramic.

3.2.3 Thermal Energy Harvesting using AM Ceramics

The thermal energy harvesting capabilities of PZT structures fabricated through AM was characterized. Flat structures, as well as structures with fins acting as heat sinks were compared. The printed structures were subject to cyclic heating and cooling and the generated power was measured under closed circuit conditions with varying electric loads. The generated powers for both flat and finned samples are shown in figure 3.17.

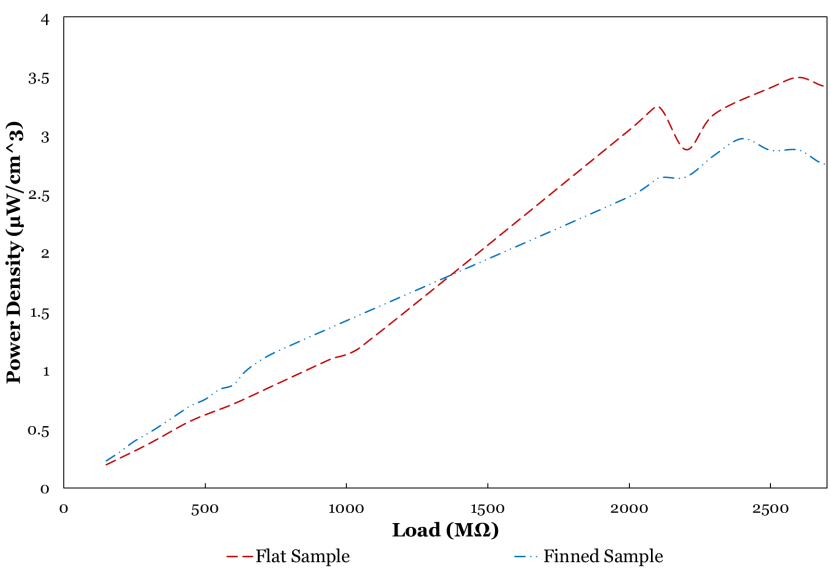

Figure 3.17. Power density of PZT structures fabricated through AM under varying electric loads.

Despite having higher power generated under low electric loads, the finned samples underperformed the flat samples at higher loads. The peak power generated was also lower for the finned samples. The advantages of fins in heat dissipation were underscored by potential fabrication defects such as interlayer porosity in the AM structures. The peak power density harvested by the PZT flat and finned samples were 3.643 and 3.034 $\mu W/cm^3$. The AM PZT structures require further characterization to understand the effects of porosities on the energy

harvesting capabilities and introduce better designs to improve the figure of merit by increasing heat dissipation or decreasing the permittivity.

Conclusion

Conventionally manufactured and AM ceramics with pyroelectric and piezoelectric properties were studied for their energy harvesting potential under combined mechanical and thermal inputs.

The performance of conventional ceramics was characterized in thermal, mechanical, and combined modes. It was found that the thermal harvesting performance of LNB ceramics varied with temperature despite being in the operational range. The ceramics exhibited highest power generation of 20.5 μW at lower temperatures despite having a lower pyroelectric coefficient than at elevated temperatures (200-225 °C). The performance of PZT ceramics under combined thermal and mechanical loads produced a lower peak power of 501 nW than purely thermal loads, which produced 494 nW. The contributions of both the pyroelectric and piezoelectric effects were out of phase because of the different rates of compression and of heating and cooling, and the competition of the dipole motions caused an overall lower power generation.

The binder jetting (BiJ) AM methods was used to build energy harvesting ceramics. BTO ceramics built using BiJ obtained sintered densities of up to 56% and high degrees of anisotropy due to the build process were observed. The ceramics were stronger and had a higher piezoelectric coupling coefficient when measured perpendicular to the printing direction. The presence of porosity in between print layers, due to the low packing density in the powder bed, contributed to lower permittivities and lower load transfer. The binder saturation used during the BiJ process positively contributed to an increase in final part density due to liquid phase sintering. However, an increase in saturation beyond 200% resulted in lower sintered densities due to increased separation between ceramic particles inhibiting sintering.

PZT ceramics were built using material extrusion (ME) AM method. The densities achieved using this method were much higher compared to those achieved through BiJ. The

thermal energy harvesting capabilities of the PZT structures fabricated through AM were superior to conventionally manufactured PZT with a harvested power density of 3.643 $\mu W/cm^3$ compared to 0.2 $\mu W/cm^3$. The addition of fins into the structure was facile and could be achieved through ME without any modification to the manufacturing process. However, the addition of fins, which were meant to increase the ratio of change in temperature, did not increase the power density of the PZT structures when compared to flat samples.

Energy harvesting ceramics show potential to power wireless MEMS sensors for long operation inside a combustion chamber. AM efforts reveal that some degree of porosity in the final parts is always present. However, porosity can result in enhanced figures of merit for energy harvesting. Precise control of the print parameters in the future will result in ceramics with enhanced harvesting capabilities that can be built with complex geometries and miniaturized for introduction into MEMS.

References

[1] "Annual Energy Outlook 2020." https://www.eia.gov/outlooks/aeo/ (accessed Dec. 16, 2020).

[2] M. R. H. Sarker *et al*., "Temperature measurements using a lithium niobate (LiNbO3) pyroelectric ceramic," *Measurement*, vol. 75, pp. 104–110, Nov. 2015, doi: 10.1016/j.measurement.2015.07.044.

[3] R. J. M. Vullers, R. v Schaijk, H. J. Visser, J. Penders, and C. V. Hoof, "Energy Harvesting for Autonomous Wireless Sensor Networks," *IEEE Solid-State Circuits Magazine*, vol. 2, no. 2, pp. 29–38, Spring 2010, doi: 10.1109/MSSC.2010.936667.

[4] D. Zabek and F. Morini, "Solid state generators and energy harvesters for waste heat recovery and thermal energy harvesting," *Thermal Science and Engineering Progress*, vol. 9, pp. 235–247, Mar. 2019, doi: 10.1016/j.tsep.2018.11.011.

[5] H.-C. Song, S.-W. Kim, H. S. Kim, D.-G. Lee, C.-Y. Kang, and S. Nahm, "Piezoelectric Energy Harvesting Design Principles for Materials and Structures: Material Figure-of-Merit and Self-Resonance Tuning," *Advanced Materials*, vol. n/a, no. n/a, p. 2002208, doi: https://doi.org/10.1002/adma.202002208.

[6] T. R. Shrout and S. J. Zhang, "Lead-free piezoelectric ceramics: Alternatives for PZT?," *J Electroceram*, vol. 19, no. 1, pp. 113–126, Sep. 2007, doi: 10.1007/s10832-007-9047-0.

[7] G. A. Smolenskii, N. N. Krainik, N. P. Khuchua, V. V. Zhdanova, and I. E. Mylnikova, "The Curie Temperature of LiNbO3," *physica status solidi (b)*, vol. 13, no. 2, pp. 309–314, 1966, doi: https://doi.org/10.1002/pssb.19660130202.

[8] "Porous ferroelectrics for energy harvesting applications | SpringerLink." https://link.springer.com/article/10.1140/epjst/e2015-02600-y (accessed Dec. 16, 2020).

[9] A. Zocca, P. Colombo, C. M. Gomes, and J. Günster, "Additive Manufacturing of Ceramics: Issues, Potentialities, and Opportunities," *Journal of the American Ceramic Society*, vol. 98, no. 7, pp. 1983–2001, 2015, doi: https://doi.org/10.1111/jace.13700.

[10] A. A. Zadpoor, "Mechanical meta-materials," *Mater. Horiz.*, vol. 3, no. 5, pp. 371–381, 2016, doi: 10.1039/C6MH00065G.

[11] H. Cui *et al*., "Three-dimensional printing of piezoelectric materials with designed anisotropy and directional response," *Nature Materials*, vol. 18, no. 3, Art. no. 3, Mar. 2019, doi: 10.1038/s41563-018-0268-1.

[12] C. R. Bowen, A. Perry, A. C. F. Lewis, and H. Kara, "Processing and properties of porous piezoelectric materials with high hydrostatic figures of merit," *Journal of the European Ceramic Society*, vol. 24, no. 2, pp. 541–545, Jan. 2004, doi: 10.1016/S0955-2219(03)00194-8.

[13] "Characterization of ceramic components fabricated using binder jetting additive manufacturing technology | Elsevier Enhanced Reader." https://reader.elsevier.com/reader/sd/pii/S0272884216302127?token=0B4AFF44CC51DADC40F36F5AAB0FB3288CC0F86069FEC06E5970E516AC4763C60789D9F9457D72FD629E24A98173D041 (accessed Dec. 16, 2020).

[14] S. B. Lang, L. H. Rice, and S. A. Shaw, "Pyroelectric Effect in Barium Titanate Ceramic," p. 7.

[15] "BaTiO3-based piezoelectrics: Fundamentals, current status, and perspectives: Applied Physics Reviews: Vol 4, No 4." https://aip.scitation.org/doi/full/10.1063/1.4990046 (accessed Dec. 16, 2020).

[16] J. A. Lewis, J. E. Smay, J. Stuecker, and J. Cesarano, "Direct Ink Writing of Three-Dimensional Ceramic Structures," *Journal of the American Ceramic Society*, vol. 89, no. 12, pp. 3599–3609, 2006, doi: https://doi.org/10.1111/j.1551-2916.2006.01382.x.

[17] B. A. Tuttle *et al.*, "Robocast Pb(Zr0.95Ti0.05)O3 Ceramic Monoliths and Composites," *Journal of the American Ceramic Society*, vol. 84, no. 4, pp. 872–874, 2001, doi: https://doi.org/10.1111/j.1151-2916.2001.tb00756.x.

[18] M. Safar, T. W. Button, and M. Zabcik, "Control of PbO loss during sintering of PZT: Laboratory vs industry," in *2017 Joint IEEE International Symposium on the Applications of Ferroelectric (ISAF)/International Workshop on Acoustic Transduction Materials and Devices (IWATMD)/Piezoresponse Force Microscopy (PFM)*, May 2017, pp. 83–88, doi: 10.1109/ISAF.2017.8000218.

[19] J. E. Marion, C. H. Hsueh, and A. G. Evans, "Liquid-Phase Sintering of Ceramics," *Journal of the American Ceramic Society*, vol. 70, no. 10, pp. 708–713, 1987, doi: https://doi.org/10.1111/j.1151-2916.1987.tb04868.x.